The Canadian Mineralogist
Vol. 44, pp. 1513-1528 (2006)

TEXTURES AND COMPOSITIONAL VARIABILITY IN GERSDORFFITE FROM THE CRESCENCIA Ni–(Co–U) SHOWING, CENTRAL PYRENEES, SPAIN: PRIMARY DEPOSITION OR RE-EQUILIBRATION?

ISABEL FANLO[§] AND IGNACIO SUBÍAS

Cristalografía y Mineralogía, Departamento de Ciencias de la Tierra, Universidad de Zaragoza, C/ Pedro Cerbuna 12, E–50009 Zaragoza, Spain

FERNANDO GERVILLA

Instituto Andaluz de Ciencias de la Tierra y Departamento de Mineralogía y Petrología, Facultad de Ciencias, C.S.I.C.–Universidad de Granada, E–18002 Granada, Spain

JOSE MANUEL

Cristalografía y Mineralogía, Departamento de Ciencias de la Tierra, Universidad de Zaragoza, C/ Pedro Cerbuna 12, E–50009 Zaragoza, Spain

ABSTRACT

At the Crescencia showing in the Pyrenees, Spain, three stages of mineral deposition can be distinguished: stage I: nickeline and pararammelsbergite, stage II: gersdorffite, and stage III: uraninite. Gersdorffite has been subdivided into seven groups on the basis of textural and compositional criteria. Some of these groups of gersdorffite clearly show disequilibrium processes that may have been induced by secondary reactions associated with a re-equilibration of the system during cooling. Formation and subsequent growth of gersdorffite nuclei on the nickeline (0001) surface, self-organization, or a coupled dissolution-and-reprecipitation moving interface through pararammelsbergite or nickeline are some of the processes invoked during the re-equilibration. Thus, the compositional variations found in the seven groups of gersdorffite are likely due to intermediate steps during the bulk of the replacement and re-equilibration processes at low temperature, rather than a direct precipitation from the ore-forming fluids under different conditions.

Keywords: gersdorffite, nickeline, pararammelsbergite, uraninite, mineral replacement, dissolution–precipitation, recrystallization front, reaction rims, self-organization, Pyrenees, Spain.

SOMMAIRE

A l'indice minéralisé de Crescencia, dans les Pyrénées espagnoles, nous distinguons trois stades de déposition du minerai: Stade I: nickeline et pararammelsbergite, stade II: gersdorffite, et stade III: uraninite. La gersdorffite est subdivisée en sept groupes selon des critères texturaux et compositionnels. Certains de ces groupes de gersdorffite mettent clairement en évidence un déséquilibre, dû peut-être à des réactions secondaires associées à un ré-équilibrage du système au cours du refroidissement. La formation et la croissance de nucléi de gersdorffite sur la surface (0001) de la nickeline, une auto-organisation, et un front de dissolution et reprécipitation couplées traversant la pararammelsbergite ou la nickeline seraient des processus possibles invoqués lors du ré-équilibrage. Les variations en composition que nous documentons parmi les sept groupes de gersdorffite témoigneraient de stades intermédiaires au cours des processus de remplacement et de ré-équilibrage à faible température, plutôt que de précipitation directe à partir des fluides formateurs du minerai à de diverses conditions.

(Traduit par la Rédaction)

Mots-clés: gersdorffite, nickeline, pararammelsbergite, uraninite, remplacement de minéraux, dissolution–reprécipitation, front de recristallisation, couronnes de réaction, auto-organisation, Pyrénées, Espagne.

§ *E-mail address*: fanlo@unizar.es

Introduction

In the foothills of the Pyrenees belt in northeastern Spain, we have found two groups of small-scale Ni–Co deposits hosted by metasomatized Paleozoic limestones, depending on whether Co or Ni is dominant: cobalt is dominant in the San Juan de Plan deposit studied by Fanlo *et al*. (2004), whereas nickel is dominant at the Crescencia showing, the subject of this communication.

Deposits of Ni–Co ore minerals are widespread, and they have been extensively studied in the literature. Recent investigations have focused on the compositional variations in sulfarsenides, arsenides and diarsenides, with studies of natural compositional trends, bonding models and schemes of coupled substitution, and descriptions of the phase relations involving the solid solutions at high temperatures (Yund 1962, Klemm 1965, Petruk *et al*. 1971, Maurel & Picot 1974, Ixer *et al*. 1979, Fukuoka & Hirowatari 1980, Oen *et al*. 1984, Béziat *et al*. 1996, Gervilla *et al*. 1996, Hem *et al*. 2001, Wagner & Lorenz 2002, Hem & Makovicky 2004, Fanlo *et al*. 2004).

In general, the influence of mineral replacement as a consequence of re-equilibration processes is not considered as a major process in explaining the composition of minerals. In this paper, we focus on textures and compositional variations of gersdorffite at the Crescencia showing. These features may provide evidence for a series of re-equilibration processes at low temperature, rather than a direct precipitation from the ore-forming fluids of different composition under distinct conditions of temperature.

Geology of the Deposit

The Crescencia showing is located in the central part of the Pyrenees (longitude 42°31'53.8" N, and latitude 00°34'17.5" E), a doubly verging collisional mountain belt that resulted from the interaction between the Ibero-African and European plates in Mesozoic and Cenozoic times. Even now, the Ibero-African plate margin is converging at a rate of 4 mm/year.

The oldest rocks in the area comprise a monotonous sequence of sedimentary rocks of Cambrian–Ordovician age. Pre-Variscan augen gneisses and granitic gneisses occur as elongate east–west domes surrounded by Variscan aureoles. An overlying Devonian sequence consists of grey limestone and shale, locally calcareous. These rocks are conformably overlain by Carboniferous chert, nodular limestone and, unconformably, by dark shale and flysch sequences. Batholiths of granodiorite were emplaced in the Paleozoic rocks. Triassic redbeds lie unconformably on the Hercynian basement, with a basal conglomerate horizon filling an erosional surface. Limestones of Cretaceous age rest unconformably on the Triassic redbeds or directly on the basement. These limestones have been strongly deformed during Alpine thrusting and locally possess a mylonitic fabric.

The Crescencia ore is hosted by limestone of the early Devonian sequence, which alternates with black shale. This ore-bearing unit is extensively dolomitized. The deposit consists of a horizontal east–west-striking vein, 50 m long and 10 cm wide, located along the contact between the limestone and black shale. An irregular and discordant zone of disseminated mineralization occurs along the vein. The Hercynian structure of both host rocks and ore is disrupted by an east–west Alpine thrust fault verging to the south. The deposit is not obviously related to an intrusive body. Nickel was extracted from artisanal workings toward the end of the 19th century and the beginning of the 20th century.

Mineralogy and Petrography

The mineral assemblage at the Crescencia showing is characterized by Ni sulfarsenides, arsenides and diarsenides, together with late uraninite. The gangue minerals consist of ankerite and dolomite.

Three stages of mineral deposition can be distinguished on the basis of mineralogical and textural studies: Stage I: nickeline (NiAs, Nc) and pararammelsbergite ($NiAs_2$, Prr); Stage II: gersdorffite (ideally NiAsS, Gdf), and Stage III: uraninite (UO_2, Urn). The black shales adjacent to the vein contain a dissemination of pyrite (Py) rimmed by gersdorffite, although a relation between these minerals in the shale and in the vein assemblage is not evident.

Stage I comprises masses of allotriomorphic-granular aggregates of nickeline, showing a random orientation and variable grain-size. The nickeline shows a distinct (0001) cleavage and, occasionally, an incipient lamellar twinning. In some crystals, this lamellar twinning is made more prominent by alteration or destabilization of the grains (Fig. 1A). Pararammelsbergite occurs as roundish, poorly developed crystals included in nickeline or along the contact between nickeline and gersdorffite. The pararammelsbergite does not show twinning and exhibits rotation tints rich in various shades of brown. Both nickeline and pararammelsbergite are found as remnants of resorption in gersdorffite.

Stage II is dominated by gersdorffite, which overgrows or replaces grains of nickeline and fills small cracks in them. We recognize seven groups of gersdorffite on the basis of mode of occurrence and compositional variability. The groups are named gersdorffite A, B, C, D, E and F throughout the text, tables and figures. The black-shale-hosted gersdorffite overgrowing pyrite crystals is described as gersdorffite G.

Euhedral grains of *gersdorffite A*, generally of small size (<20 μm), are scattered in the masses of nickeline (Fig. 1B), or aligned among the grains of nickeline (Figs. 1C, D). Along the contact between the relics of

nickeline and the euhedral gersdorffite, resorbed remains of pararammelsbergite are observed. As the euhedral crystals replaced nickeline and, locally, pararammelsbergite, they coalesced, growing outward and leading to irregular and inhomogeneous masses of gersdorffite enclosing the relics of nickeline and pararammelsbergite (Fig. 1E). *Gersdorffite B* consists of small irregular crystals with complex twinning (Fig. 1F); under crossed nicols, all the crystals are optically isotropic. *Gersdorffite C* also replaces nickeline and pararammelsbergite, forming a rhythmic development of reaction rims; the rims are irregularly distributed and closely spaced with respect to each other (Figs. 1G, H). *Gersdorffite D* forms homogeneous masses of coarse, subhedral aggregates; it occasionally contains inclusions of nickeline or pararammelsbergite (Fig. 1I). *Gersdorffite E* consists of irregular patches of As-rich gersdorffite in contact with masses of nickeline. Far from the interface between nickeline and gersdorffite E, the patches become smaller until they practically vanish. In these zones, gersdorffite D predominates (Fig. 1I). Euhedral crystals of *gersdorffite F* are included in nickeline, and they show irregular growth-bands (Fig. 1J). *Gersdorffite G* consists of euhedral crystals overgrowing the pyrite grains disseminated in the black shales close to the vein (Fig. 1K).

Stage-III mineralization is characterized by the deposition of uraninite following a recrystallization front affecting both nickeline and gersdorffite (Fig. 1L). Texturally, uraninite forms concentric structures of a few micrometers across (5–10 μm), which may coalesce and produce tabular aggregates. In some cases, these aggregates grow along crystallographic directions of gersdorffite crystals (Fig. 1M). The uraninite seems unaltered, and where the crystals are observed with both reflected-light microscopy and SEM, they do not display variations in brightness, which are characteristic of homogeneous compositions and indicative of absence of alteration or recrystallization (Fayek *et al*. 2002).

Analytical Methods

Fifteen samples were studied by reflected-light microscopy, electron-probe micro-analysis and X-ray diffraction (XRD), and back-scattered-electron images were used to characterize textural features of the samples. X-ray powder-diffraction studies were carried out using a Philips PW–1729 diffractometer with a monochromatic Cu*K*α radiation and equipped with an X-ray-diffraction analysis program (Martin 2004). Chemical compositions of the Ni-bearing minerals were determined by wavelength-dispersion electron-probe micro-analysis using a CAMECA SX–50 instrument at the University of Barcelona. The ore minerals were analyzed for Fe, Co, Ni, Sb, As and S; the elements Cu, Bi, Zn, Pt and Pd were found to be below the detection limit. We monitored the peaks Fe*K*α, Co*K*α, Ni*K*α, S*K*α, As*L*α, Sb*L*α, Cu*K*α, Zn*K*α, Bi*L*α, and Pb*M*α. Operating conditions included an accelerating voltage of 20 kV and a beam current of 20 nA. The counting times were 20 s on TAP/PET and 30 s on LiF crystals. ZAF corrections were performed using the program supplied by CAMECA. Pyrite, GaAs, NiO, as well as pure Co metal were used as primary standards. Chemical compositions of uraninite samples were established using an accelerating voltage of 20 kV and a beam current of 100 nA in order to increase counts. Peaks were counted for 10 seconds on TAP/PET and LiF crystals except for Pb, for which the peak was counted for 100 seconds. We used the *M*β line for U to avoid interference from ThL , Zr*K*α, Fe*K*α and Pβb lines. The *K*α lines were used for Si, Ca, P, Mg, Al, K, Mn, Ti and Fe; the *L*α for Y, and Zr, and *M*α for Th and Pb. We used as standards synthetic UO_2, ThO_2, ZrO_2, $CaMO_4$, InAs and minerals (orthoclase for K, Al and Si, apatite for P, galena for Pb, rutile for Ti, spessartine for Mn). The proportion of oxygen was obtained by stoichiometry. The maximum, minimum, mean and representative results of the point analyses in the grains numbered in Figures 1, 2 and 3 are given below in tables.

Composition of the Minerals

Nickeline and pararammelsbergite (*Stage I*)

Results of electron-microprobe analyses (Table 1) of nickeline reveal a nearly stoichiometric composition:

FIG. 1. Representative textures of ore minerals from the Crescencia showing. All photomicrographs are back-scattered-electron images, except Figures 1C, D and E (reflected-light images). The numbers indicate sites of spot micro-analyses; the relevant compositions are presented in Tables 1 to 6. Symbols: Nc: nickeline; Gdf A to G: the seven different types of gersdorffite from stage II; Prr: pararammelsbergite, Py: pyrite, Urn: uraninite. (A) Anhedral aggregates of nickeline showing a cleavage (black areas) parallel to (0001) along which replacement has proceeded. (B) Euhedral crystals of gersdorffite A scattered in the masses of nickeline. (C) Crystals of gersdorffite A aligned along grain boundaries of nickeline. (D) Same photomicrograph as (C) under polarized light. (E) Growth and coalescence of gersdorffite A nuclei in nickeline masses. (F) Crystals of gersdorffite B showing complex twinning. (G) Nickeline crystals hosting minute inclusions of pararammelsbergite, partially replaced by gersdorffite C, which form rhythmically zoned reaction-rims. (H) Enlarged image of the left bottom of the Figure 2E showing the irregular distribution of the rims. (I) Irregular patches of gersdorffite E along the interface nickeline–gersdorffite; far from this recrystallization front, gersdorffite D is dominant. (J) Euhedral crystals of gersdorffite F marked by irregular growth-bands included in nickeline. (K) Euhedral crystal of gersdorffite G overgrows the pyrite grain disseminated in the black shale. (L) A recrystallization front of uraninite affecting both gersdorffite and nickeline. (M) The uraninite crystals occur as spheres and, locally, can be seen to grow along crystallographic directions in gersdorffite.

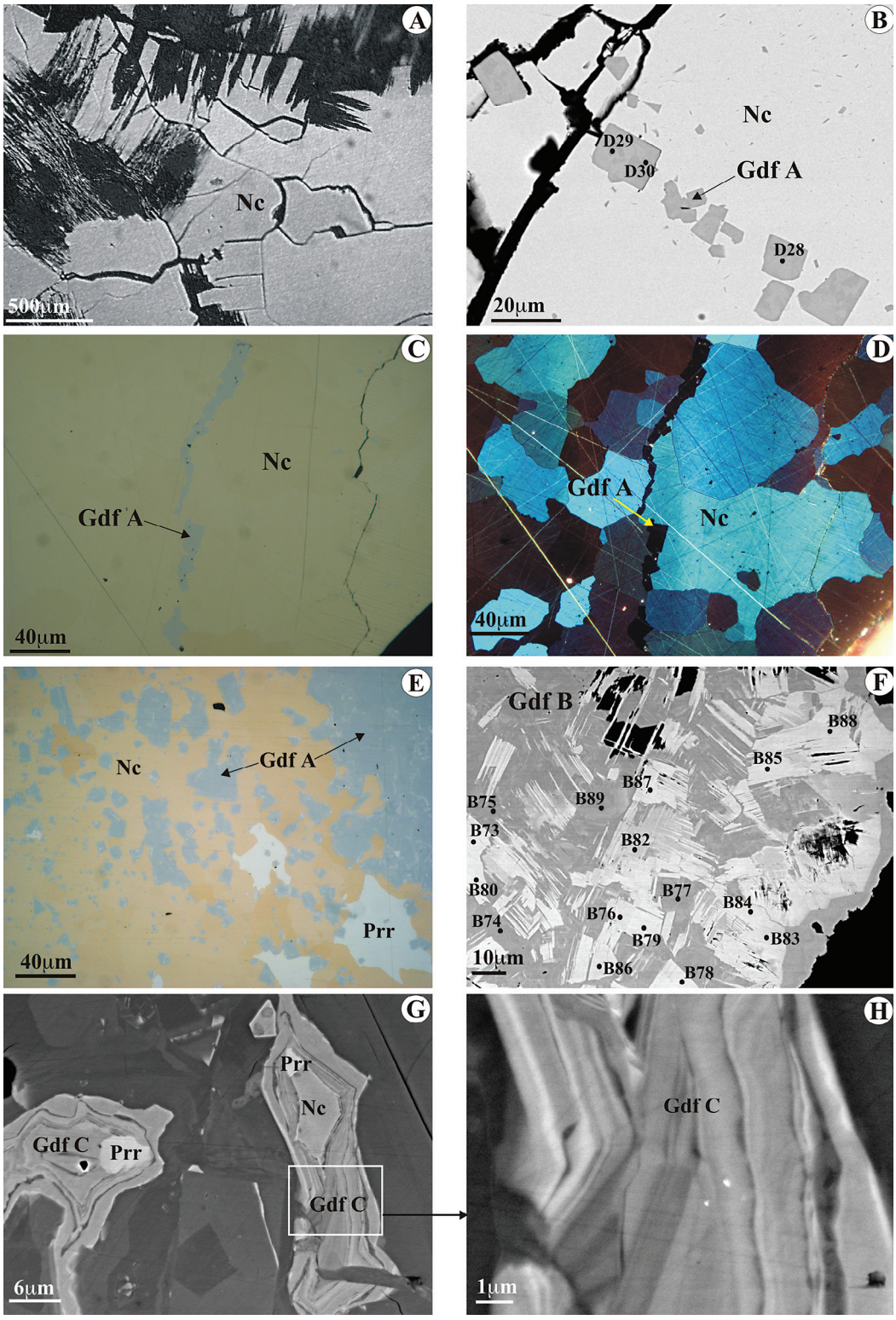
A
Nc
500μm
B
Nc
D29
D30
Gdf A
D28
20μm
C
Nc
Gdf A
40μm
D
Gdf A
Nc
40μm
E
Nc
Gdf A
Prr
40μm
F
Gdf B
B88
B85
B87
B89
B75
B73
B82
B80
B77
B84
B74
B76
B79
B83
B86
B78
10μm
G
Prr
Nc
Gdf C
Prr
Gdf C
6μm
H
Gdf C
1μm

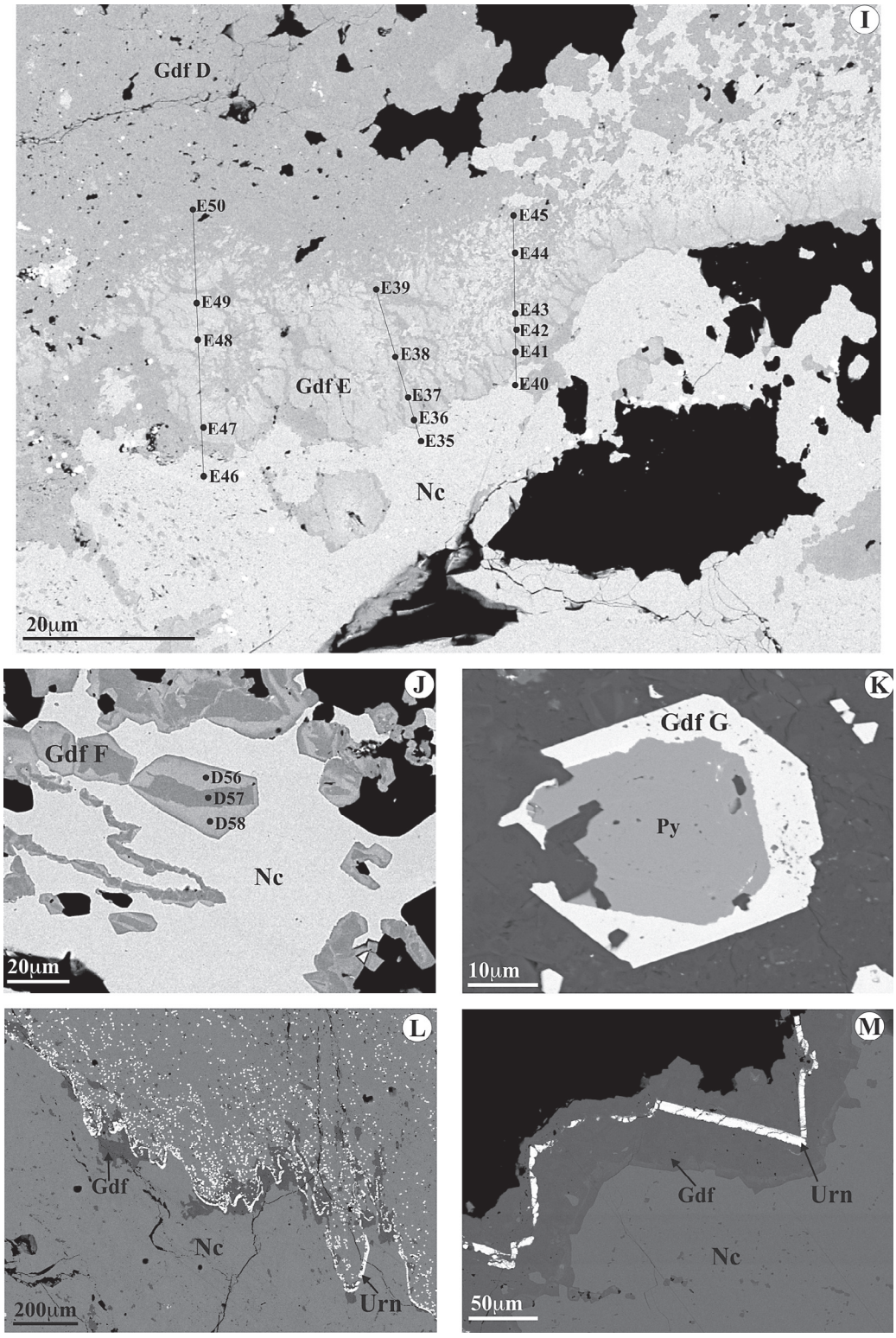
I
Gdf D
E50
E49
F48
E47
E46
E39
E38
Gdf E
E37
E36
E35
E45
E44
E43
E42
E41
E40
Nc
20μm
J
Gdf F
D56
D57
D58
Nc
20μm
K
Gdf G
Py
10μm
L
Gdf
Nc
Urn
200μm
M
Gdf
Urn
Nc
50μm

TABLE 1. STATISTICAL RESULTS OF ELECTRON-MICROPROBE ANALYSES OF NICKELINE AND PARARAMMELSBERGITE FROM THE CRESCENCIA SHOWING, CENTRAL PYRENEES, SPAIN

		Compositions (weight %)							Atoms per formula unit						
		S	As	Sb	Fe	Co	Ni	Total	S	As	Sb	Fe	Co	Ni	As:S
Nc	min	0.00	54.19	0.00	0.00	0.00	42.10	100.48	0.00	0.97	0.00	0.00	0.00	0.98	-
n = 70	max	1.92	57.38	2.57	0.35	0.18	44.15	99.41	0.08	1.02	0.03	0.01	0.00	1.01	-
	mean	0.14	56.01	0.57	0.03	0.04	43.12	99.78	0.00	1.00	0.00	0.00	0.00	0.98	-
Prr	min	0.03	70.91	0.00	0.00	0.00	26.71	99.00	0.00	1.94	0.00	0.00	0.00	0.96	-
n = 21	max	0.66	72.28	0.87	0.10	0.44	29.05	100.80	0.04	2.01	0.02	0.00	0.02	1.01	-
	mean	0.24	71.59	0.41	0.02	0.06	27.84	99.94	0.02	1.99	0.01	0.00	0.01	0.98	-

$Ni_{0.98–1.01}Fe_{0–0.01}As_{0.97–1.02}Sb_{0–0.03}S_{0–0.08}$. The composition of pararammelsbergite (Table 1) lies within the range $Ni_{0.96–1.01}Co_{0–0.02}As_{1.94–2.01}Sb_{0–0.02}S_{0–0.04}$. The S content in pararammelsbergite falls within the range established experimentally by Yund (1962).

Gersdorffite (*Stage II*)

Gersdorffite shows a compositional variability depending on its mode of occurrence. Over 275 spot analyses were made of the seven types of gersdorffite. The general formula corresponds to $(Ni_{0.57–1.05}Co_{0–0.39}Fe_{0–0.12})As_{0.97–1.65}Sb_{0–0.07}S_{0.37–1.01}$; however, there are substantial differences among the seven types. The As:S ratio spans a wide range, from 0.96 to 4.46. (1.61 ± 0.83). Most crystals of gersdorffite show a As:S ratio greater than the ideal As:S, 1; they are devoid of Fe (except for gersdorffite G), and devoid of Co (types C, D and E).

Gersdorffite A (cubic crystals included in nickeline) exhibits the following compositional variability: $(Ni_{0.80–1.01}Co_{0–0.18})As_{1.01–1.55}Sb_{0–0.05}S_{0.40–0.99}$ (Table 2); the As:S ratio ranges from 1.03 to 3.88 (1.44 ± 0.84). There is a strong negative correlation between As and S (R = –0.99); however, there is no correlation between anion and cation proportions. Cobalt also is present in variable contents (from 0 to 6.61 wt%). The contents of As and Co are highly variable within a single grain (Fig. 1B, Table 2) and are inhomogeneous in their distribution.

Gersdorffite B (twinned crystals) is characterized by highly variable As and S contents among the different lamellae (Fig. 1F, Table 2). The As:S ratio ranges from 1.13 to 4.23 (2.97 ± 1.18) and displays contents of Co higher than in the other types of gersdorffite (from 3.00 to 7.43 wt.%), except for gersdorffite G. Its composition is $(Ni_{0.78–0.88}Co_{0.10–0.22})As_{1.07–1.65}Sb_{0–0.02}S_{0.39–0.95}$ (Table 2). The As:S variability is directly related to the Ni and Co contents, as there are positive correlations between As and Ni (R = 0.87) and, between S and Co (R = 0.88) (Fig. 2).

Gersdorffite C (reactions rims) displays the highest contents of As and Ni. The As:S ratio ranges between 1.82 to 4.46 (2.96 ± 0.56) (Table 3). Its composition is $Ni_{0.99–1.01}As_{1.29–1.65}Sb_{0–0.02}S_{0.37–0.71}$. Both gersdorffite B and C show As values very close to the maximum As content determined experimentally by Yund (1962). Only gersdorffite from San Juan de Plan (Fanlo *et al.* 2004) displays a higher content (66.29 wt% As) than that at the Crescencia mine (maximum 63.90 wt% As). Gersdorffite at both ore deposits spans the broad range in As:S ratios found in the literature although, as will be explained below, their respective conditions of formation are clearly different. As can be seen in Table 3 and Figures 3A–D, the inner rim of gersdorffite C (Fig. 3C, anal. 39, 49, 50, 51 and 53), in contact with the core of pararammelsbergite, displays a higher As content than next to the nickeline cores (Figs. 3B, D). The Co and Fe contents are the lowest of all the different types.

Gersdorffite D (massive) is the most abundant and homogeneous type, showing the As and S values closest to the ideal composition: $(Ni_{0.91–1.00}Co_{0–0.05}Fe_{0–0.03})As_{0.97–1.17}Sb_{0–0.07}S_{0.83–1.01}$. The As:S ratio varies between 0.98 and 1.40 (1.09 ± 0.08). The Co and Fe contents are very low, below 1.73 wt% Co and 1.12 wt% Fe (Table 4).

Gersdorffite E consists of very irregular patches enriched in As (up to 57.50 wt%) where they are close to the masses of nickeline. As can be seen in Figure 1I and Table 4, however, far away from these masses, the patches have a composition similar to those of gersdorffite D (45.73 wt % As). The general composition is $(Ni_{0.94–1.01}Co_{0–0.05}Fe_{0–0.02})As_{1.04–1.43}Sb_{0.02}S_{0.54–0.94}$. The As:S ratio varies between 1.11 and 2.65 (1.77 ± 0.52).

Gersdorffite F (euhedral crystals with growth bands) displays values of arsenic slightly lower than in gersdorffite A (Table 5). The general composition is: $(Ni_{0.84–1.00}Co_{0–0.15}Fe_{0–0.05})As_{1.01–1.37}Sb_{0–0.03}S_{0.64–0.99}$,

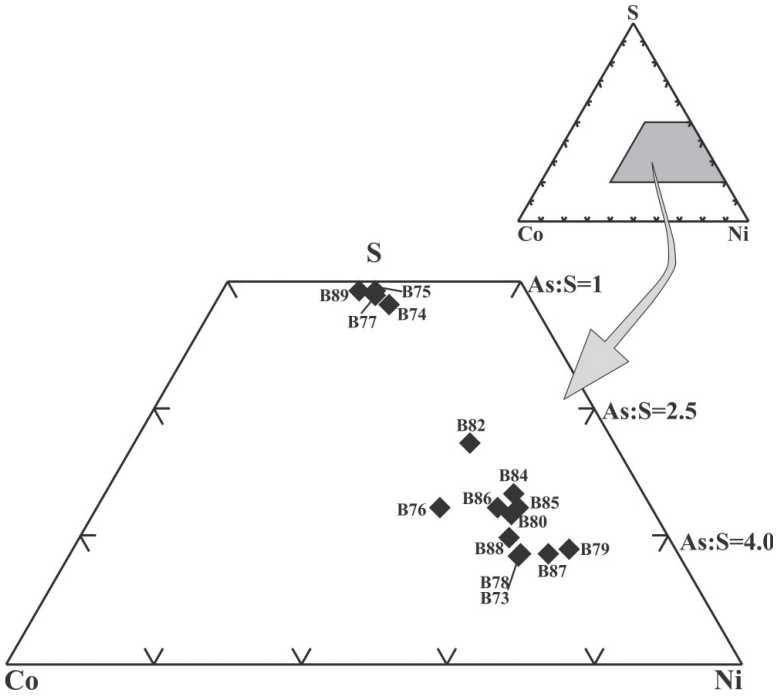

FIG. 2. Triangular plot showing the correlation between S and Co and Ni contents, in gersdorffite B, in atoms per formula unit. The numbers refer to the spot micro-analyses; compositions are listed in Table 2 and indicated in Figure 1D.

with a As:S ratio ranging between 1.02 and 2.11 (1.49 ± 0.32). The inner bands of the idiomorphic crystals commonly display the highest S contents, whereas the outer bands, in contact with the masses of nickeline, show the highest As values (Fig. 1J); this variation is not accompanied by variations in metal contents.

Gersdorffite G (overgrowth on pyrite crystals) shows the highest Co, Fe and lowest As contents and is the only Sb-free gersdorffite: $(Ni_{0.57–0.78}Co_{0.18–0.39}Fe_{0.02–0.12})As_{0.97–1.10}S_{0.90–1.01}$. The As:S ratio is in the range of 0.96–1.21 (1.11 ± 0.07) (Table 5).

Uraninite (*Stage III*)

The minimum, maximum and mean results of 20 electron-microprobe analyses of the uraninite found at the Crescencia showing, together with the calculated formula and the U–Pb chemical ages, are given in Table 6. U–Pb chemical ages of uraninite were calculated from the U, Th and Pb contents determined by electron-probe micro-analysis using the method of Bowles (1990). The chemical age is based on the assumption that the total Pb present in the sample is of radiogenic origin, the result of the decay of U and Th; the larger ionic radius of the Pb^{2+} (1.37 Å) compared with U^{4+} (1.05 Å) and their difference in valence preclude a straightforward incorporation of Pb into the structure of uraninite. The accuracy of analyses for Pb by the electron microprobe is ±0.1%, which results in errors of 10 Ma in the chemical ages. We have used the empirical formula of Ranchin (1968), which is best adapted for ages less than 200 Ma. As the sum of all oxides from EMPA (Σ) is invariably less than 100 wt%, Σ_1 has been recalculated taking into account the excess of normalized cations (Σcat) and the number of oxygen ions (Σox) needed to compensate for them. An amount of U^{4+} has been converted to U^{6+} to compensate for Pb plus Ca (*cf.* Alexandre & Kyser 2005).

The uraninite grains show lead contents varying from 0.80 to 1.52 wt% PbO and have incorporated minor Ca, Ti, Si, Th, Y and Fe. Elements such as P, Zr, Mg, Mn and the rare-earth elements (REE) are low or below the detection limit, which is approximately 0.2 wt% (Table 6).

The increase in SiO_2, CaO and FeO with decreasing age of uraninite, with a moderate negative correlation (R = –0.70) (Fig. 4), suggests that uraninite underwent alteration by fluid-circulation events, and that this alteration occurred on a microscale. During this alteration process, uraninite may have been variably recrystallized, incorporating Ca, Si and Fe in some way (Fayek *et al.* 1997). However, taking into account

TABLE 2. STATISTICAL RESULTS OF ELECTRON-MICROPROBE ANALYSES OF GERSDORFFITE A AND B FROM THE CRESCENCIA SHOWING, CENTRAL PYRENEES, SPAIN

	Compositions (weight %)							Atoms per formula unit						
	S	As	Sb	Fe	Co	Ni	Total	S	As	Sb	Fe	Co	Ni	As:S
Gdf A min	6.72	44.88	0.14	0.00	0.00	28.31	99.70	0.40	1.01	0.00	0.00	0.00	0.80	1.03
n = 12 max	18.79	60.64	3.33	0.02	6.61	34.12	101.60	0.99	1.55	0.05	0.00	0.18	1.01	3.88
mean	16.38	48.53	1.23	0.00	1.56	32.47	100.90	0.87	1.12	0.02	0.00	0.06	0.95	1.44
D28	17.73	47.19	1.77	0.00	1.42	33.35	101.6	0.93	1.06	0.02	0.00	0.03	0.96	1.14
D29	18.61	44.88	1.65	0.00	0.48	34.08	99.7	0.98	1.01	0.02	0.00	0.02	0.98	1.03
D30	17.22	46.96	1.86	0.00	2.63	32.06	100.7	0.91	1.06	0.03	0.00	0.07	0.93	1.16
Gdf B min	6.35	46.69	0.15	0.02	3.00	24.25	99.15	0.39	1.07	0.00	0.00	0.10	0.78	1.13
n = 24 max	17.90	63.64	0.98	0.29	7.43	27.66	100.82	0.95	1.65	0.02	0.02	0.22	0.88	4.23
mean	10.02	57.95	0.41	0.10	5.11	25.97	99.61	0.57	1.45	0.00	0.00	0.16	0.82	2.97
B73	6.44	63.22	0.40	0.03	4.55	25.16	99.80	0.39	1.63	0.00	0.00	0.15	0.83	4.18
B74	17.16	47.69	0.15	0.10	6.39	27.66	99.15	0.93	1.07	0.00	0.00	0.19	0.81	1.15
B75	17.82	47.52	0.27	0.13	7.00	26.87	99.61	0.95	1.07	0.00	0.00	0.02	0.78	1.13
B76	7.98	60.68	0.46	0.04	6.22	24.25	99.63	0.47	1.54	0.00	0.00	0.21	0.78	3.28
B77	17.55	47.14	0.35	0.05	7.31	26.86	99.26	0.94	1.07	0.00	0.00	0.20	0.79	1.14
B78	6.88	62.77	0.39	0.04	4.49	26.25	100.82	0.40	1.59	0.00	0.00	0.15	0.85	3.98
B79	6.66	63.15	0.33	0.10	3.00	26.88	100.12	0.40	1.62	0.00	0.00	0.10	0.88	4.05
B80	7.51	61.52	0.34	0.07	4.39	25.38	99.21	0.45	1.59	0.00	0.00	0.14	0.83	3.53
B82	9.91	58.18	0.42	0.29	4.67	26.08	99.55	0.57	1.44	0.00	0.02	0.15	0.81	2.53
B83	7.55	61.18	0.51	0.09	4.60	25.26	99.19	0.46	1.57	0.00	0.00	0.15	0.82	3.41
B84	8.34	59.62	0.47	0.12	4.21	26.17	98.93	0.49	1.52	0.00	0.00	0.13	0.85	3.10
B85	7.65	60.96	0.98	0.19	4.02	25.87	99.67	0.46	1.55	0.02	0.00	0.13	0.85	3.37
B86	7.77	61.00	0.61	0.08	4.83	25.47	99.76	0.46	1.55	0.02	0.00	0.15	0.82	3.37
B87	6.35	63.64	0.21	0.04	3.76	26.05	100.05	0.39	1.65	0.00	0.00	0.12	0.87	4.23
B88	6.85	62.68	0.44	0.02	4.87	24.86	99.72	0.41	1.63	0.00	0.00	0.15	0.84	3.98
B89	17.9	47.21	0.22	0.14	7.43	26.49	99.39	0.95	1.07	0.00	0.00	0.22	0.78	1.13

The sites of the spot micro-analyses are indicated in Figures 1B and 1F.

that the circulation of fluids enhances the alteration of uraninite, leading to a loss of lead contents and a decrease in the total concentration of oxides, this alteration under oxidizing conditions was limited in the Crescencia deposit and relatively localized, because the analytical totals are relatively high (from 95 to 98 wt%, Table 6).

Discussion

Conditions of ore formation

The nickeline – (para)rammelsbergite – gersdorffite assemblage is a common association in some ore deposits. Commonly, these minerals are intimately intergrown, or show complex textural and compositional variations, reflecting an environment of rapid fluctuations in temperature as well as in chemical activities (Oen *et al*. 1984, Choi & Imai 1985, Choi & Youm 2000, Wagner & Lorenz 2002, Power *et al*. 2004, Fanlo *et al*. 2004). The As:S ratio and cation contents have been used to distinguish the different variants of gersdorffite in high-temperature deposits. Moreover, Hem *et al*. (2001), Hem & Makovicky (2004) and (Fanlo *et al*. (2004) have suggested that both As and Ni contents in the gersdorffite–cobaltite solid solution are controlled by the fugacity of As in the mineralizing fluid at high temperature.

Other Ni–Co deposits hosted by Paleozoic limestones in the Pyrenees, such as the San Juan de Plan deposit, indicate temperatures of formation of approximately 600°C, as deduced from phase relations (Fanlo *et al*. 2004). The solvus diagram of Klemm (1965) is not applicable to systems that show extensive substitutions and disequilibrium textures. However, as gersdorffite G does not seem to display As-for-S substitution (As:S ratio in the range of 0.96–1.21) or re-equilibration, we plot these data in the system NiAsS–CoAsS–FeAsS (Klemm 1965). Gersdorffite G, with the highest content of Co, indicates a temperature of deposition around 400°C (Fig. 5). The other types of gersdorffite may have formed at lower temperatures; the extent of solid solution involving Ni and Co is very limited at low temperatures (<300°C), as documented by Hem & Makovicky (2004).

Bayliss (1982) described three structural variants of gersdorffite, and suggested their dependence on temperature: $P2_13$ is the low-temperature form, $Pa3$ is the high-temperature form, and $Pca2_1$ is an intermediate and metastable form. The last form is characterized by

TABLE 3. STATISTICAL RESULTS OF ELECTRON-MICROPROBE ANALYSES OF GERSDORFFITE C AND THE POINT ANALYSES FROM FIGURE 3

	Compositions (weight %)							Atoms per formula unit						
	S	As	Sb	Fe	Co	Ni	Total	S	As	Sb	Fe	Co	Ni	As:S
Gdf C min	6.04	54.18	0.00	0.00	0.00	29.54	98.81	0.37	1.29	0.00	0.00	0.00	0.99	1.82
n = 40 max	12.97	63.90	0.81	0.10	0.10	33.08	100.73	0.71	1.65	0.02	0.00	0.00	1.00	4.46
mean	8.85	59.75	0.15	0.01	0.02	31.17	99.92	0.52	1.49	0.00	0.00	0.00	0.99	2.96
1 Gdf D	18.93	46.43	1.00	0.00	0.00	33.72	100.08	0.99	1.01	0.02	0.00	0.00	0.99	1.05
2 Gdf D	18.28	46.55	1.08	0.10	0.10	34.01	100.12	0.96	1.02	0.02	0.00	0.00	0.99	1.08
3 Gdf C	10.19	58.54	0.00	0.00	0.10	31.38	100.21	0.59	1.44	0.00	0.00	0.00	0.99	2.44
4 Nc	1.24	55.07	0.10	0.10	0.10	43.54	100.15	0.05	0.97	0.00	0.00	0.00	0.98	-
5 Nc	0.00	56.00	0.20	0.10	0.00	43.91	100.21	0.00	1.00	0.00	0.00	0.00	1.00	-
6 Nc	1.43	54.67	0.15	0.00	0.00	43.43	99.63	0.05	0.97	0.00	0.00	0.00	0.98	-
7 Gdf C	8.93	60.38	0.00	0.10	0.10	30.29	99.80	0.52	1.51	0.00	0.00	0.00	0.99	2.9
8 Gdf D	18.83	45.76	0.00	0.00	0.00	34.58	99.17	0.99	1.02	0.00	0.00	0.00	0.99	1.03
9 Gdf D	19.10	45.90	0.00	0.00	0.00	34.16	99.16	1.00	1.01	0.00	0.00	0.00	0.99	1.01
10 Gdf D	19.06	45.82	0.10	0.10	0.10	34.90	100.08	0.99	1.01	0.00	0.00	0.00	0.99	1.03
26 Gdf D	19.18	45.00	0.93	0.00	0.00	34.84	99.95	1.00	1.00	0.02	0.00	0.00	0.98	1.00
27 Gdf D	17.05	48.19	0.00	0.00	0.00	34.56	99.80	0.90	1.09	0.00	0.00	0.00	1.01	1.21
28 Gdf C	8.00	61.02	0.00	0.00	0.00	30.76	99.78	0.47	1.54	0.00	0.00	0.00	0.99	3.28
29 Gdf C	9.24	59.37	0.00	0.00	0.00	31.69	100.30	0.54	1.46	0.00	0.00	0.00	1.00	2.70
30 Prr	0.48	71.10	0.00	0.00	0.00	27.95	99.53	0.02	1.98	0.00	0.00	0.00	1.00	-
31 Prr	2.70	68.20	0.00	0.00	0.00	28.63	99.53	0.16	1.84	0.00	0.00	0.00	0.99	-
32 Gdf C	9.22	59.02	0.00	0.00	0.00	31.64	99.88	0.54	1.46	0.00	0.00	0.00	1.00	2.70
33 Gdf C	8.42	60.92	0.00	0.00	0.00	30.93	100.27	0.49	1.52	0.00	0.00	0.00	0.99	3.10
34 Gdf D	18.13	46.63	0.00	0.00	0.00	34.72	99.49	0.96	1.04	0.00	0.00	0.00	0.99	1.08
37 Gdf D	18.42	46.36	0.00	0.00	0.00	34.72	99.51	0.96	1.04	0.00	0.00	0.00	0.99	1.08
38 Gdf C	9.20	59.27	0.00	0.00	0.00	31.42	99.89	0.54	1.46	0.00	0.00	0.00	1.00	2.70
39 Gdf C	7.58	61.29	0.00	0.00	0.00	30.27	99.14	0.46	1.56	0.00	0.00	0.00	0.99	3.39
40 Prr	1.55	70.14	0.00	0.00	0.00	29.05	100.74	0.10	1.91	0.00	0.00	0.00	0.99	-
41 Prr	1.32	70.63	0.00	0.00	0.00	28.54	100.49	0.08	1.92	0.00	0.00	0.00	1.00	-
42 Gdf C	7.56	60.95	0.00	0.00	0.00	30.87	99.38	0.46	1.54	0.00	0.00	0.00	1.01	3.35
43 Gdf C	10.03	57.94	0.00	0.00	0.00	31.44	99.41	0.57	1.43	0.00	0.00	0.00	1.00	2.51
44 Gdf D	18.10	46.03	1.01	0.00	0.00	34.54	99.68	0.95	1.03	0.02	0.00	0.00	1.00	1.08
45 Gdf D	18.77	44.92	0.00	0.00	0.00	34.75	98.44	0.99	1.01	0.00	0.00	0.00	0.99	1.02
47 Gdf D	17.47	47.80	0.00	0.00	0.00	34.67	99.94	0.92	1.08	0.00	0.00	0.00	1.00	1.17
48 Gdf C	8.01	61.01	0.00	0.00	0.00	31.00	100.02	0.47	1.53	0.00	0.00	0.00	1.00	3.26
49 Gdf C	7.45	61.60	0.00	0.00	0.00	30.85	99.90	0.44	1.56	0.00	0.00	0.00	1.01	3.55
50 Gdf C	7.98	60.60	0.00	0.00	0.00	30.85	99.43	0.47	1.53	0.00	0.00	0.00	1.00	3.26
51 Gdf C	6.92	63.00	0.00	0.00	0.00	30.88	100.90	0.42	1.58	0.00	0.00	0.00	1.00	3.76
52 Gdf C	9.02	59.53	0.00	0.00	0.00	31.40	99.95	0.53	1.48	0.00	0.00	0.00	0.99	2.79
53 Gdf C	7.46	61.25	0.00	0.00	0.00	30.85	99.56	0.44	1.56	0.00	0.00	0.00	1.01	3.55
54 Gdf C	10.04	57.99	0.00	0.00	0.00	31.99	100.02	0.57	1.43	0.00	0.00	0.00	1.00	2.51
55 Gdf D	18.25	46.05	0.00	0.00	0.00	34.92	99.22	0.97	1.03	0.00	0.00	0.00	1.00	1.06
56 Gdf D	18.64	46.12	0.00	0.00	0.00	34.98	99.74	0.97	1.03	0.00	0.00	0.00	1.00	1.03
57 Gdf D	19.25	45.15	0.00	0.00	0.00	35.30	99.70	1.00	1.00	0.00	0.00	0.00	1.00	1.00
58 Gdf C	8.72	59.31	0.00	0.00	0.00	31.37	99.40	0.51	1.49	0.00	0.00	0.00	1.00	2.92
59 Gdf C	12.55	54.35	0.00	0.00	0.00	33.08	99.98	0.70	1.30	0.00	0.00	0.00	1.00	1.86
60 Nc	0.00	56.01	0.00	0.00	0.00	43.93	99.94	0.00	1.00	0.00	0.00	0.00	1.00	-
62 Nc	0.00	56.10	0.00	0.00	0.00	43.75	99.85	0.00	1.00	0.00	0.00	0.00	1.00	-
64 Nc	0.69	55.01	0.00	0.00	0.00	43.92	99.62	0.03	0.97	0.00	0.00	0.00	1.00	-
65 Gdf C	9.49	58.52	0.00	0.00	0.00	31.60	99.61	0.56	1.44	0.00	0.00	0.00	1.00	2.57
66 Gdf D	18.04	46.81	0.00	0.00	0.00	34.86	99.71	0.95	1.05	0.00	0.00	0.00	1.00	1.11
67 Nc	0.00	55.89	0.00	0.00	0.00	43.83	99.72	0.00	1.00	0.00	0.00	0.00	1.00	-
69 Nc	0.05	55.79	0.00	0.00	0.00	43.30	99.14	0.00	1.00	0.00	0.00	0.00	1.00	-
70 Gdf C	12.97	54.18	0.00	0.00	0.00	32.76	99.91	0.71	1.29	0.00	0.00	0.00	1.00	1.82
71 Gdf C	10.79	56.63	0.00	0.00	0.00	32.21	99.63	0.62	1.38	0.00	0.00	0.00	1.00	2.23
72 Gdf C	9.74	58.19	0.00	0.00	0.00	31.79	99.72	0.56	1.44	0.00	0.00	0.00	1.00	2.57
73 Gdf C	10.37	57.59	0.00	0.00	0.00	32.01	99.97	0.59	1.41	0.00	0.00	0.00	1.01	2.39
74 Gdf C	9.17	58.91	0.00	0.00	0.00	31.54	99.62	0.54	1.46	0.00	0.00	0.00	1.00	2.70
75 Gdf C	9.50	58.79	0.00	0.00	0.00	31.90	100.19	0.56	1.44	0.00	0.00	0.00	1.00	2.57
76 Gdf D	17.74	47.08	0.00	0.00	0.00	34.79	99.61	0.93	1.07	0.00	0.00	0.00	1.00	1.15

The sites of the spot micro-analyses are indicated in Figures 3B, 3C, and 3D.

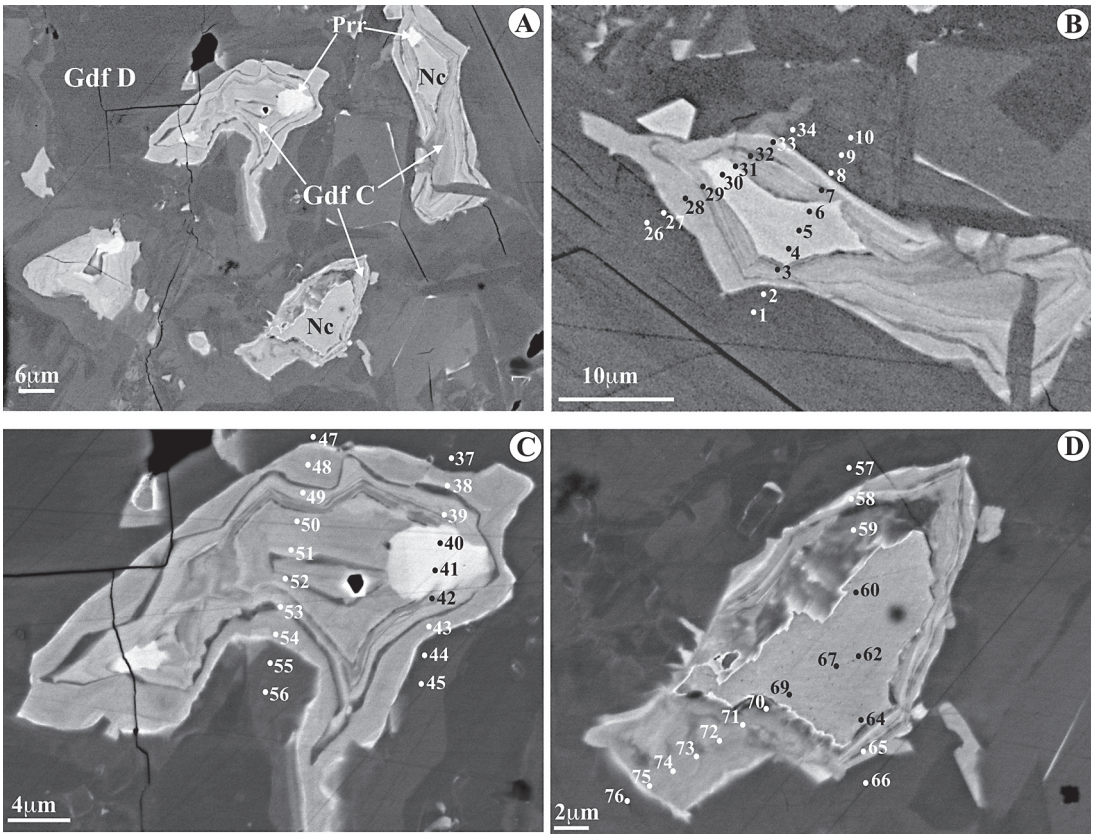

FIG. 3. (A) Back-scattered-electron images showing crystals of gersdorffite C. All the spot analyses are referenced in Table 3. (B) Enlarged image of a gersdorffite C crystal replacing nickeline (anal. 1 to 10, Table 3) and a small grain of pararammelsbergite (anal. 26 to 34). (C) Enlarged image to show the various reaction-fronts. The spot analyses located in the same rim and closest to pararammelsbergite (*e.g.,* anal. 39 and 49) display similar compositions and are richer in As than those farther away from the core (*e.g.,* anal. 43 and 54). (D) The reaction rims around the nickeline core are partially altered, which may be due to a re-equilibration of gersdorffite C, which leads to a S enrichment (*cf.* anal. 58 and 59).

the presence of complex twins, high Co and Fe contents and the presence of the reflections 010 and 110 in the powder-diffraction pattern, whereas the $P2_13$ form is characterized by the reflection 110. In his heating experiments, Bayliss (1982) determined a structural change at 550° and 600°C with the loss of the 010 reflection first, and then the loss of the 110 reflection. With respect to the twinned crystals of gersdorffite B, if they were to represent the metastable gersdorffite, with space group $Pca2_1$, the diffraction patterns would show the 010 and 110 reflections. However, only the reflection 110, corresponding to the ordered phase $P2_13$ is present, which would indicate that the "twins" are not the result of a transformation twinning.

Taking into account the complex textures and the pronounced variations in As found in gersdorffite at the Crescencia showing, a question arises. Are the textures and compositional variability the result of a primary precipitation and, therefore, a consequence of variations in temperature and solution composition, or are they the result of re-equilibration processes?

Are the textural features acquired during primary deposition or by re-equilibration?

In general, the replacement of one mineral phase by another implies the role of a fluid phase, its interaction with the rock (or mineral), and therefore, the fluid: rock ratio is a variable. For instance, the introduction of a fluid with a higher activity of sulfur results in the destabilization of nickeline and the formation of gersdorffite.

From a compositional and textural point of view, a simple process of primary precipitation cannot explain

TABLE 4. STATISTICAL RESULTS OF ELECTRON-MICROPROBE ANALYSES OF GERSDORFFITE D and E AND THE POINT ANALYSES OF FIGURE 1I

		Compositions (weight %)							Atoms per formula unit						
		S	As	Sb	Fe	Co	Ni	Total	S	As	Sb	Fe	Co	Ni	As:S
Gdf D	min	15.50	45.15	0.12	0.00	0.00	31.06	98.96	0.83	0.97	0.00	0.00	0.00	0.91	0.98
n =	max	19.25	50.56	4.92	1.12	1.73	35.09	101.90	1.01	1.17	0.07	0.03	0.05	1.00	1.40
126	mean	17.96	45.79	1.60	0.11	0.14	33.65	99.27	0.95	1.04	0.02	0.00	0.00	0.98	1.09
Gdf E	min	9.32	45.73	0.74	0.08	0.03	30.55	98.56	0.54	1.04	0.02	0.00	0.00	0.94	1.11
n = 12	max	17.85	57.50	1.71	0.45	1.53	34.66	100.53	0.94	1.43	0.02	0.02	0.05	1.01	2.65
	mean	13.33	52.02	1.20	0.25	0.82	32.20	99.77	0.74	1.24	0.02	0.01	0.03	0.98	1.77
	E35	0.21	54.60	1.17	0.01	0.02	44.63	100.64	0.02	1.45	0.02	0.00	0.00	1.51	-
	E36	10.96	54.69	1.30	0.18	1.30	31.35	99.78	0.63	1.34	0.02	0.00	0.04	0.98	2.13
	E37	14.61	49.89	1.44	0.33	1.01	31.28	98.56	0.81	1.18	0.02	0.02	0.04	0.94	1.46
	E38	13.18	52.47	1.22	0.32	0.78	32.55	100.52	0.73	1.24	0.02	0.02	0.02	0.98	1.7
	E39	17.72	45.73	1.13	0.08	0.03	34.59	99.28	0.94	1.04	0.02	0.00	0.00	1.01	1.11
	E40	0.06	56.03	0.61	0.04	0.07	43.01	99.82	0.00	1.51	0.02	0.00	0.00	1.47	-
	E41	11.31	54.91	0.74	0.21	1.53	31.31	100.01	0.64	1.33	0.02	0.00	0.05	0.96	2.08
	E42	12.12	54.04	1.00	0.14	1.28	31.51	100.09	0.68	1.29	0.02	0.00	0.04	0.97	1.9
	E43	13.35	51.32	1.37	0.34	1.10	32.16	99.64	0.75	1.21	0.02	0.02	0.04	0.98	1.61
	E44	0.28	55.71	0.68	0.05	0.08	43.45	100.25	0.02	1.48	0.02	0.00	0.00	1.48	-
	E45	17.85	46.10	1.71	0.09	0.12	34.66	100.53	0.94	1.04	0.02	0.00	0.00	0.99	1.11
	E46	0.58	54.50	0.93	0.04	0.04	43.06	99.22	0.04	1.47	0.02	0.00	0.00	1.47	-
	E47	9.32	57.26	0.97	0.32	0.79	30.56	99.46	0.54	1.43	0.02	0.02	0.02	0.97	2.65
	E48	9.89	54.00	1.06	0.45	0.92	30.55	100.13	0.57	1.40	0.02	0.02	0.04	0.96	2.46
	E49	11.95	46.32	1.32	0.20	0.86	31.38	99.71	0.68	1.32	0.02	0.00	0.02	0.97	1.94
	E50	17.65	54.81	1.11	0.33	0.14	34.52	100.07	0.93	1.04	0.02	0.02	0.00	0.99	1.12

The sites of the spot micro-analyses are indicated in Figure 1I.

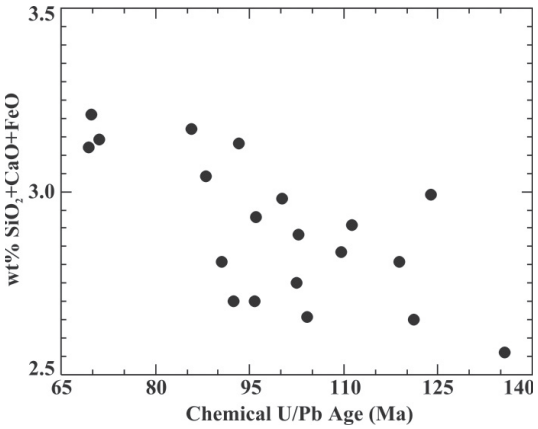

FIG. 4. Relationship between SiO_2 + CaO + FeO contents and chemical U–Pb ages of uraninite from the Crescencia showing (data from Table 6).

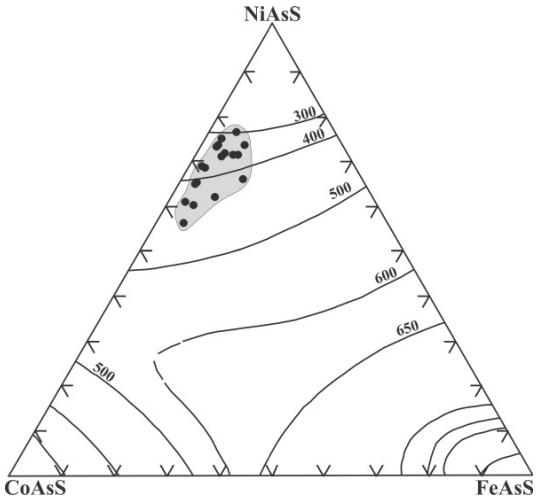

FIG. 5. Compositional plot of the gersdorffite G in the system NiAsS–CoAsS–FeAsS. Solvus lines at different temperatures are taken from Klemm (1965).

most types of gersdorffite that we find. Rather, mineral-replacement processes, chemical self-organization and changes in the sulfur fugacity $f(S_2)$ of the fluids should be invoked. With respect to gersdorffite A, its formation may be consistent with a destabilization of nickeline in the presence of pervasive fluids with high $f(S_2)$. Thus, the formation of a high proportion of nuclei and subsequent growth arose in the masses

of nickeline (Figs. 1B, E). This process is similar to that reported by Pina *et al*. (2000) for the dissolution of the (001) face of phosgenite, with the formation of two types of etch pits, and the subsequent nucleation of cerussite crystals on the (001) surface. Inasmuch as the gersdorffite nuclei are expected to grow on the (0001) surface of nickeline, they undersaturate the fluids with respect to As and maintain its continued dissolution. This feedback process would be consistent with a stationary non-equilibrium state where the formation and growth of gersdorffite nuclei are constant, whereas the nickeline is far from equilibrium. Fletcher & Merino (2001) suggested that the force of crystallization associated with the growth of new crystals causes pressure dissolution of the host phase, allowing space for the replacement to take place. In both cases, the presence of gersdorffite on the surface of nickeline may affect the local diffusion-gradients in the fluid in contact with both phases (Pina *et al*. 2000).

With regard to gersdorffite B, if the twins had been the result of a structural change from a high (cubic) to a low (orthorhombic) form, the diffraction patterns should show the 010 and 110 reflection typical of gersdorffite $Pca2_1$ (Bayliss 1982). However, only the 110 reflection is observed, which is indicative of a $P2_13$ form. Moreover, the high variability in the contents of As of the different crystals of the twinned assemblage (>13 wt%) runs against the expectations of an inversion-induced twin. Notwithstanding, one might consider that fluids with a high $f(S_2)$ penetrated along the cleavage (0001) or, occasionally, along the incipient lamellar twinning in nickeline, as can be seen in Figure 1A (compare this figure with Fig. 1F). As fluids penetrate along these directions, nickeline was replaced and the precipitation of As-enriched lamellae of gersdorffite was enhanced (Fig. 1F). If so, the lamellar twins in gersdorffite B were inherited from the nickeline crystals; a similar process was described by Holness (2003) during the replacement of K-feldspar by albite.

The textures showed by gersdorffite C resemble those described by Oen *et al*. (1984) from the Franklin deposit, New Jersey. They suggested that variations in mineral composition in gersdorffite and rammelsbergite rims, due to variations in the composition of solutions and degree of supersaturation at the interface, were the result of diffusion-controlled chemical gradients. However, although gersdorffite replaced rammelsbergite or nickeline, there was no substitution of As-for-S in the gersdorffite rims. Figures 3B–D and Table 3 show that the rims of gersdorffite are more As-enriched if the core is pararammelsbergite instead of nickeline. Far from the reaction rims, gersdorffite C did re-equilibrate, showing nearly stoichiometric proportions of arsenic and sulfur. Thus, the arsenic-rich rim in gersdorffite may be the product of leaching of arsenic (and nickel) from pararammelsbergite and nickeline, and a reaction with the residual solutions, enriched in sulfur. As equilibrium was attained, gersdorffite began to show an As:S ratio closer to 1, similar to those values displayed by gersdorffite D (anal. 1, 2, 8–10, 26, 27, 34, 37, 44, 45, 47, 55, 56, 57, 66 and 76 from Figs. 3B–D). Therefore, these reaction rims are likely to represent a replacement-induced reaction-front, moving through the pararammelsbergite or nickeline. Similar results were attained in experiments by Geisler *et al*. (2001) and encountered in studies of natural zircon by Tomaschek *et al*. (2001). In these studies, the reaction proceeded from the surface of the parent, and a sharp reaction-induced interface moved into the parent crystal, resulting in a pseudomorphic replacement. The reaction rims were found to be strongly enriched in some elements (as the As is in our case).

Gersdorffite types E and F represent an intermediate compositional situation with respect to types B, C and D (As:S ratio ≈ 1). Gersdorffite E resulted from a mineral-replacement reaction, which proceeds *via* a moving interface (Fig. 1I). The separation of As-enriched gersdorffite and nickeline by an interface suggests a coupled dissolution–reprecipitation process, rather than one controlled by diffusion or simple anion-exchange (Putnis 2002). Direct observations of this type of reaction on a molecular scale by AFM (Pina *et al*. 2000) showed that the rate of dissolution of the parent phase is enhanced by the nucleation of the product and by the porosity generated. Putnis (2002) suggested that the formation of porosity during such replacement reactions and the migration of cations through this fluid-filled pore-space allow the replacement to proceed. However, the replacive gersdorffite is nonporous, perhaps because the change in molar volume of the solids is positive, as the following reaction would indicate:

$$NiAs_{(Nc)} + H_2S + 1/2O_2 \rightarrow NiAsS_{(Gdf)} + H_2O \quad (1)$$

The molar volumes of nickeline and gersdorffite are 17.15 and 27.11 cm^3/mol, respectively. Therefore, the replacement of nickeline by gersdorffite on a mol-by-mol basis through reaction (1) would result in a volume increase of 58%, which would prevent the formation of porosity.

Gersdorffite F likely formed during the latter stages of evolution of gersdorffite A, once the cubic crystals had grown and coalesced. Following Ortoleva (1990) and Dewers & Ortoleva (1990), both the textures and composition of gersdorffite F may be explained in the framework of a self-organization theory: "the spontaneous transition of a non-equilibrium system from a non-patterned state to a patterned state without the intervention of a patterned external cause" (Chadam & Ortoleva 1990). In other words, a coupling between mechanical forces, chemical reactions and solute transport necessarily involves disequilibrium, feedback loops and noise (fluctuations).

Since the basis for the self-organization involves the enhancement of compositional perturbations through some type of destabilizing feedback-type mechanism,

the dissolution of nickeline and pararammelsbergite may be invoked. Consequently, this dissolution–precipitation mechanism could lead to the compositional self-organization in gersdorffite F, promoting As-rich areas close to the nickeline interface and stoichiometric bands (As:S close to 1) in the core of the crystals (Fig. 1J, Table 5).

Conclusions

From a compositional point of view, we outline two different groups of gersdorffite (Fig. 6), one with high value of the As:S ratio (types B and C), or the highest content of Co (type G), and another (types A, D, E and F) with an overlap in composition. This compositional variability of gersdorffite seems to be the result of intermediate steps during the processes of re-equilibration at low temperature, rather than a direct precipitation from the ore-forming fluids under distinct conditions of composition and temperature.

The destabilization of the (0001) surface of nickeline, due to pervasive fluids with high $f(S_2)$, led to the initial formation of gersdorffite nuclei (type A). We believe that the subsequent growth and coalescence of these cubic crystals, which had an inhomogeneous distribution of As, led to a compositional self-organization during the latter stages of evolution (gersdorffite F). Arsenic-rich gersdorffite of types B, C and E (the patches closest to nickeline) may represent the first products during the replacement process of nickeline (or pararammelsbergite in some cases of type C). Inasmuch as gersdorffite E attained chemical equilibrium, a reduction in arsenic content was produced in the patches far from the interface with the nickeline. In the formation of gersdorffite F, a destabilizing feedback-type mechanism, such as dissolution–precipitation, seems to have led to compositional self-organization in gersdorffite. Finally, As:S values close to 1 indicate that gersdorffite equilibrated with residual solutions (type D). The replacement process proceeded *via* crystallographic directions (type B) or a moving interface (types C and E).

Clearly, it is important to attempt to look deeply into the microtextural relations among minerals in ore deposits in order to detect signs of re-equilibration processes, which leads to changes in composition. These processes are common in ore deposits, and they must be identified to prevent erroneous interpretations.

Acknowledgements

Paul G. Spry and the reviewers are acknowledged for their comments, which contributed to the improvement of the original manuscript. The authors are indebted to Robert F. Martin for his help and constructive comments during the developing of the paper. This project was financially supported by the Ministerio de Ciencia y Tecnolog¡a (CGL2004–05055/BTE).

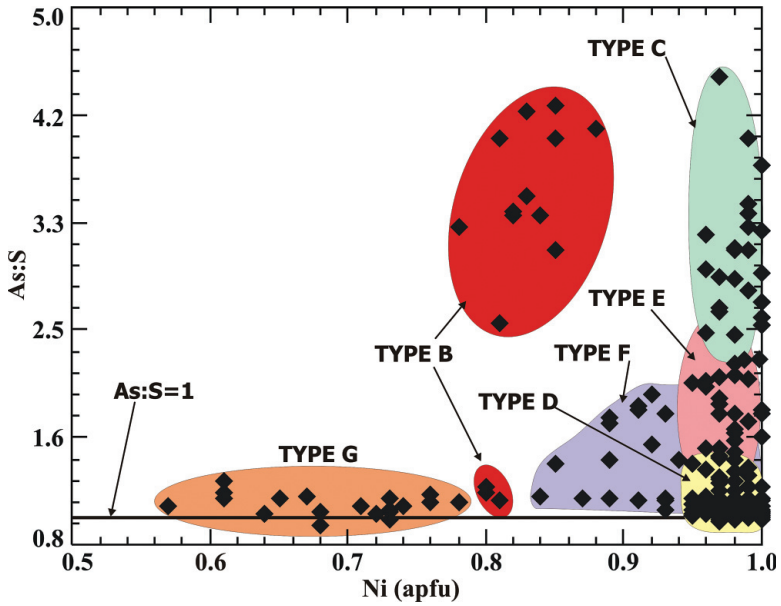

Fig. 6. As:S ratio *versus* Ni (in atoms per unit formula) of gersdorffite types from the Crescencia showing. The compositional area of Gersdorffite A has not been drawn, as it partially overlaps the areas of types D and F.

TABLE 5. STATISTICAL RESULTS OF ELECTRON-MICROPROBE ANALYSES OF GERSDORFFITE F AND G

		Compositions (weight %)							Atoms per formula unit						
		S	As	Sb	Fe	Co	Ni	Total	S	As	Sb	Fe	Co	Ni	As:S
Gdf F	min	11.53	45.70	0.09	0.01	0.05	29.31	99.12	0.64	1.01	0.00	0.00	0.00	0.84	1.02
n = 44	max	19.09	57.06	2.08	1.45	5.14	33.99	100.99	0.99	1.37	0.03	0.05	0.15	1.00	2.11
	mean	15.20	51.26	0.76	0.32	0.97	32.38	100.26	0.82	1.18	0.01	0.01	0.03	0.96	1.49
	D56	12.73	52.78	0.68	0.15	0.34	32.58	99.26	0.71	1.29	0.02	0.00	0.02	0.97	1.82
	D57	16.23	49.85	0.81	0.01	0.69	33.29	100.88	0.86	1.14	0.02	0.00	0.02	0.98	1.33
	D58	11.53	55.06	0.51	0.13	0.48	31.75	99.46	0.65	1.37	0.00	0.00	0.02	0.97	2.11
Gdf G	min	16.70	44.44	0.09	0.83	6.46	19.75	99.21	0.90	0.97	0.00	0.02	0.18	0.57	0.96
n = 17	max	19.66	48.54	0.43	4.16	13.80	26.72	100.79	1.01	1.10	0.00	0.12	0.39	0.78	1.21
	mean	19.04	46.80	0.24	1.69	9.20	24.05	100.07	0.95	1.05	0.00	0.05	0.26	0.69	1.11

The sites of the spot micro-analyses are indicated in Figure 1J.

TABLE 6. STATISTICAL RESULTS OF ELECTRON-MICROPROBE ANALYSES OF URANINITE FROM THE CRESCENCIA SHOWING, CENTRAL PYRENEES, SPAIN

	Compositions (weight %)												U–Pb chem. age
	UO_2	PbO	CaO	TiO_2	SiO_2	ThO_2	Y_2O_3	FeO	Σ	Σcat	Σox	Σ1	Ma
min	88.44	0.80	1.97	0.76	0.27	0.17	0.34	0.18	94.90	34.72	67.99	97.55	70
max	91.90	1.52	2.74	1.32	0.71	0.50	0.54	0.58	98.33	35.06	68.30	101.30	135
mean	90.66	1.07	2.29	1.01	0.40	0.36	0.44	0.33	96.92	34.83	68.10	99.76	100
	91.10	1.39	2.07	1.26	0.29	0.37	0.42	0.29	97.54	34.72	67.99	100.19	121
	90.22	1.00	2.14	1.16	0.50	0.42	0.47	0.40	96.65	34.76	68.02	99.33	88
	91.12	1.07	2.27	1.04	0.45	0.30	0.46	0.41	97.51	34.82	68.09	100.35	93
	90.77	1.36	2.07	1.10	0.37	0.49	0.44	0.37	97.34	34.75	68.02	100.04	119
	91.33	1.28	2.19	1.18	0.27	0.40	0.46	0.45	97.96	34.83	68.11	100.84	111
	88.44	1.38	2.05	1.04	0.36	0.34	0.45	0.58	95.01	34.87	68.12	97.87	124
	89.03	1.52	1.97	0.88	0.28	0.27	0.45	0.31	94.90	34.76	68.04	97.56	135
	91.27	1.10	2.16	1.00	0.27	0.37	0.37	0.27	97.10	34.74	68.03	99.79	96
	91.88	1.07	2.20	1.01	0.28	0.36	0.39	0.22	97.75	34.73	68.03	100.45	92
	89.35	1.02	2.10	1.12	0.37	0.48	0.40	0.34	95.56	34.77	68.07	98.27	91
	90.59	1.19	2.09	0.99	0.31	0.45	0.37	0.26	96.61	34.72	67.99	99.23	104
	89.47	0.80	2.26	1.01	0.45	0.39	0.47	0.43	95.68	34.84	68.11	98.50	71
	90.25	1.14	2.31	1.04	0.38	0.41	0.48	0.29	96.68	34.84	68.11	99.53	100
	90.73	1.28	2.67	0.76	0.40	0.17	0.40	0.20	97.00	34.98	68.23	100.11	112
	90.47	1.35	2.74	0.81	0.49	0.24	0.48	0.22	97.20	35.06	68.33	100.50	118
	91.37	1.18	2.13	0.88	0.29	0.40	0.44	0.33	97.40	34.76	68.04	100.13	102
	91.89	1.11	2.33	0.89	0.35	0.41	0.34	0.25	97.89	34.80	68.09	100.72	96
	91.60	0.80	2.52	0.80	0.42	0.20	0.44	0.18	97.19	34.87	68.14	100.11	70
	90.95	0.80	2.48	0.83	0.42	0.21	0.48	0.31	96.72	34.91	68.18	99.70	70
	91.60	0.99	2.31	1.05	0.44	0.40	0.35	0.42	97.92	34.80	68.05	100.72	86

apfu	U	Pb	Ca	Ti	Si	Th	Y	Fe	U^{4+}	U^{6+}
min	0.792	0.008	0.088	0.023	0.011	0.001	0.007	0.007	0.663	0.103
max	0.825	0.017	0.117	0.038	0.028	0.005	0.011	0.020	0.720	0.130
mean	0.808	0.012	0.098	0.030	0.016	0.003	0.009	0.011	0.698	0.110

Σ: The sum of all oxides from EMPA data. Σcat: normalized cations. Σox: normalized number of oxygen. Σ1: sum of all oxides recalculated taking into account Σcat and Σox.

References

BAYLISS, P. (1982): A further crystal structure refinement of gersdorffite. *Am. Mineral.* **67**, 1058- 1064.

BÉZIAT, D., MONCHOUX, P. & TOLLON, F. (1996): Cobaltite–gersdorffite solid solution as a primary magmatic phase in spessartite, Lacaune area, Montagne Noire, France. *Can. Mineral.* **34**, 503-512.

BOWLES, J.F.W. (1990): Age dating of individual grains of uraninite in rocks from electron microprobe analyses. *Chem. Geol.* **83**, 47-53.

CAUS, E., TEIXELL, A. & BERNAUS, J.M. (1997): Depositional model of a Cenomanian–Turonian extensional basin (Sopeira Basin, NE Spain): interplay between tectonics, eustasy and biological productivity. *Paleogeog. Palaeoclimatol. Palaeoecol.* **129**, 23-36.

CHADAM, J. & ORTOLEVA, P. (1990): Morphological instabilities in physico-chemical systems. *Earth Sci. Rev.* **29**, 175-181.

CHOI, SEON-GYU & IMAI, N. (1985): Ni–Fe–Co arsenides and sulfarsenides from the Ulsan mine, Republic of Korea. *Mining Geol.* **35**, 1-16.

CHOI, SEON-GYU & YOUM, SEUNG-YOUM (2000): Compositional variation of arsenopyrite and fluid evolution at the Ulsan deposit, southeastern Korea: a low-sulfidation porphyry system. *Can. Mineral.* **38**, 567-584.

DEWERS, T. & ORTOLEVA, P. (1990): Differentiated structures arising from mechano-chemical feedback in stressed rocks. *Earth Sci. Rev.* **29**, 283-298.

FANLO, I., SUBÍAS, I., GERVILLA, F., PANIAGUA, A. & GARCÍA, B. (2004): The composition of Co–Ni–Fe sulfarsenides, diarsenides and triarsenides from the San Juan de Plan deposit, central Pyrenees, Spain. *Can. Mineral.* **42**, 1221-1240.

FAYEK, M., JANECZEK, J. & EWING, R.C. (1997): Mineral chemistry and oxygen isotopic analyses of uraninite, pitchblende and uranium alteration minerals from the Cigar Lake deposit, Saskatchewan, Canada. *Appl. Geochem.* **12**, 549-565.

FAYEK, M., KYSER, T.K. & RICIPUTI, L.R. (2002): U and Pb isotope analyses of uranium minerals by ion microprobe and the geochronology of the McArthur River and Sue zone uranium deposits, Saskatchewan, Canada. *Can. Mineral.* **40**, 1553-1569.

FLETCHER, R.C. & MERINO, E. (2001): Mineral growth in rocks: kinetic-rheological models of replacement, vein formation and syntectonic crystallization. *Geochim. Cosmochim. Acta* **65**, 3733-3748.

FUKUOKA, M. & HIROWATARI, F. (1980): On minerals in the system Ni–Co–As–S from the bedded manganese ore deposits in the eastern part of Yamaguchi Prefecture; on the chemical compositions of gersdorffite–cobaltite solid solution. *Sci. Rep. Fac. Sci., Kyushu Univ., Geology* **13**, 239-249.

GEISLER, T., ULONSKA, M., SCHLEIDER, H., PIDGEON, R.T. & VON BRONSWIJK, W. (2001): Leaching and differential crystallization of metamict zircon under experimental hydrothermal conditions. *Contrib. Mineral. Petrol.* **141**, 53-65.

GERVILLA, F., LEBLANC, M., TORRES-RUIZ, J. & FENOLL HACH-ALÍ, P. (1996): Immiscibility between arsenide and sulfide melts: a mechanism for concentration of noble metals. *Can. Mineral.* **34**, 485-502.

HEM, S.R. & MAKOVICKY, E. (2004): The system Fe–Co–Ni–As–S. II. Phase relations in the (Fe,Co,Ni)$As_{1.5}S_{0.5}$ section at 650° and 500°C. *Can. Mineral.* **42**, 63-86.

HEM, S.R., MAKOVICKY, E. & GERVILLA, F. (2001): Compositional trends in Fe, Co and Ni sulfarsenides and their crystal-chemical implications; results from the Arroyo de la Cueva deposits, Ronda Peridotite, southern Spain. *Can. Mineral.* **39**, 831-853.

HOLNESS, M.B. (2003): Growth and albitization of K-feldspar in crystalline rocks in the shallow crust: a tracer for fluid circulation during exhumation? *Geofluids* **3**, 89-102.

IXER, R.A., STANLEY, C.J. & VAUGHAN, D.J. (1979): Cobalt-, nickel-, and iron-bearing sulfarsenides from the north of England. *Mineral. Mag.* **43**, 389-395.

JANECZEK, J. & EWING, R.C. (1992): Structural formula of uraninite. *J. Nucl. Mater.* **190**, 128-132.

KLEMM, D.D. (1965): Synthesen und Analysen in den Dreiecksdiagrammen FeAsS–CoAsS–NiAsS und FeS_2–CoS_2–NiS_2. *Neues Jahrb. Mineral., Abh.* **103**, 205-255.

MARTIN, J.D. (2004): Using XPowder – a Software for X-Ray Powder Diffraction Analysis. http://www.xpowder.com D.L. GR 1001/04. ISBN 84–609–1497–6.

MAUREL, C. & PICOT, P. (1974): Stabilité de l'alloclasite et de la cobaltite dans les systèmes Co–As–S et Co–Ni–As–S. *Bull. Soc. fr. Minéral. Cristallogr.* **97**, 251-256.

OEN, I.S., DUNN, P.J. & KIEFT, C. (1984): The nickel-arsenide assemblage from Franklin, New Jersey: description and interpretation. *Neues Jahrb. Mineral., Abh.* **150**, 159-172.

ORTOLEVA, P.J. (1990): Role of attachment kinetic feedback in the oscillatory zoning of crystals grown from melts. *Earth Sci. Rev.* **29**, 3-8.

PETRUK, W., HARRIS, D.C. & STEWART, J.M. (1971): Characteristics of the arsenides, sulfarsenides, and antimonides. *Can. Mineral.* **11**, 150-186.

PINA, C.M., FERNÁNDEZ-DÍAZ, L., PRIETO, M. & PUTNIS, A. (2000): In situ atomic force microscope observations of a dissolution–crystallisation reaction: the phosgenite–cerussite transformation. *Geochim. Cosmochim. Acta* **64**, 215-221.

POWER, M.R., PIRRIE, D., JEDWAB, J. & STANLEY, C.J. (2004): Platinum-group element mineralization in an As-rich magmatic sulphide system, Talnostry, southwest Scotland. *Mineral. Mag.* **68**, 395-411.

PUTNIS, A. (2002): Mineral replacement reactions: from macroscopic observations to microscopic mechanism. *Mineral. Mag.* **66**, 689-708.

RANCHIN, G. (1968): Contribution à l'étude de la répartition de l'uranium à l'état de traces dans les roches granitiques saines. Les uraninites à teneur élevée du Massif de Saint-Sylvestre (Limousin – Massif Central Français). *Sci. Terre* **13**, 161-205.

TOMASCHEK, F., KENNEDY, A., VILLA, I.M. & BALLHAUS, C. (2001): Case study of metamorphic zircons from Alpine HP/LT metamorphic rocks of Syros, Cyclades, Greece. *J. Conf. Abstr.* **6**, 678.

WAGNER, T. & LORENZ, J. (2002): Mineralogy of complex Co–Ni–Bi vein mineralization, Bieber deposit, Spessart, Germany. *Mineral. Mag.* **66**, 385-407.

YUND, R.A. (1962): The system Ni–As–S; phase relations and mineralogical significance. *Am. J. Sci.* **260**, 761-782.

ZHAO, D. & EWING, R.C. (2000): Alteration products of uraninite from the Colorado Plateau. *Radiochim. Acta* **88**, 739-749.

Received July 5, 2005, revised manuscript accepted